Journal of Thermal Analysis and Calorimetry (2019) 138:4321–4329
https://doi.org/10.1007/s10973-019-08622-w

Synthesis of anisotropic $Cu_{2-x}S$-based nanostructures by thermal oxidation

A. Kusior[1] · P. Jelen[1] · J. Mazurkow[1] · P. Nieroda[1] · M. Radecka[1]

Received: 15 November 2018 / Accepted: 23 July 2019 / Published online: 7 August 2019

Abstract

Flower-like copper sulfides nanostructures were synthesized via the solvothermal route. The structural, optical and electrochemical properties of the synthesized materials were characterized by means of X-ray diffraction (XRD), scanning electron microscopy, ultraviolet–visible spectrometry and Fourier transform infrared spectroscopy (FTIR). Thermal behavior of the obtained flower-like materials was analyzed by TG, XRD and FTIR in situ measurements, over the temperature range of 25–800 °C. It was found that both shape and phase composition remain stable until the temperature reaches 200 °C. Phase transformation mechanism was discussed. During annealing, mixture of CuS and $Cu_{1.8}S$ is converted to copper sulfide hydroxides (200–500 °C) and further to CuO (700 °C and higher). Nevertheless, hierarchically porous structure is stable only to 200 °C. Applying higher temperatures affects the solubility of the material and inflicts structural damage, resulting in the formation of dense oval particles with size of 20 to 200 nm.

Keywords $Cu_{2-x}S$ · Nanostructures · Thermal oxidation · Anisotropy

Introduction

Solar energy conversion is currently one of the most promising technologies that can provide a sustainable energy source for electrical devices and chemical reactions. Photocatalytic processes gained a significant attention due to their usefulness in water splitting [1], self-cleaning surface action [2] and removal of chemical contaminants [3]. As for the latter, the presence of pollutants, especially dyes, in post-industrial wastewater poses a threat to the environment and public health [4]. Hence, the development of efficient techniques allowing the photodegradation of dyes to non-toxic components has become of great importance. Numerous photocatalysts have been taken into account, including oxides [5–7], sulfides [8–10] and nitrides [11]. Nevertheless, the efficient utilization of visible light remains a serious challenge.

Of various photocatalysts, nanostructured metal sulfides have emerged as a prominent alternative for commonly studied metal oxides. Diversified redox chemistry and stability at room temperatures combined with tunable physicochemical properties make them ideal candidates for solar energy conversion. Within this group, copper sulfides ($Cu_{2-x}S$) remain some of the most noteworthy materials. The ability of copper to change its position in the lattice and to change its oxidation state results in different values of x. So far, eight major phases have been described: covelline ($Cu_{1.00}S$), yarrowite ($Cu_{1.12}S$), spionkopite ($Cu_{1.40}S$), geerite ($Cu_{1.60}S$), anilite ($Cu_{1.75}S$), digenite ($Cu_{1.80}S$), djurleite ($Cu_{1.97}S$) and chalcocite ($Cu_{2.00}S$), and they feature different crystal structure types, namely cubic close-packing, hexagonal close-packing or a combination of hexagonal close-packing and covalent bonding of sulfur atoms [12]. Band gap values of copper sulfides range from 1.2 eV for copper-rich sulfides [13] to ~ 2.0 eV in the case of copper-deficient ones [14]. Depending on the shape, size, morphology, phase, and composition, $Cu_{2-x}S$ can exhibit unique photocatalytic performance. Their applications as adsorbents and biosensors are also particularly worth noting.

✉ A. Kusior
akusior@agh.edu.pl

[1] Faculty of Materials Science and Ceramics, AGH University of Science and Technology, al. Mickiewicza 30, 30-059 Kraków, Poland

Nanoengineering, which is based on the strong correlation between structure and properties, has become a powerful tool in the design of functional materials. Hydrothermal and solvothermal routes are currently the most useful methods for obtaining hierarchical structures with controllable primary particle assembly and pore distribution. Synergic effects of different dimensional levels [15], high specific surface area and hollow morphology provide amplified7 photocatalytic and adsorptive performance.

Recognition that anisotropy is a powerful tool for engineering the assembly of particular targeted forms has brought new excitement to the field. The design and fabrication of particles with different geometries and anisotropic material compositions have drawn a great attention in recent years [16, 17]. Their preparation remains a challenging task.

Heating $Cu_{2-x}S$ in the air should lead to the formation of copper oxides beyond a critical temperature [18–21]. However, due to the fact that copper can diffuse and easily change the oxidation state, formation of more complex structures is more probable. A fact worth noticing is that copper ions can diffuse and change their oxidation state, which makes them ideal candidates for the formation patchiness structures. Because of that particular attention must be given to their thermal properties. Oxidation processes of natural and precipitated covellite and chalcocite are well established [22–27]. It led to the formation of various copper sulfates and eventually oxides. However, strong dependence of thermal behavior on material size and morphology, especially in nanoscale, is a cause of renewed research focused on this subject [20, 28, 29]. The prospect of patchy structures formation during thermal oxidation leaves very exciting and promising way of achieving nanostructures with unique properties and variety of applications in complex processes [30, 31].

The aim of this study was to investigate the thermal behavior of flower-like copper sulfides ($Cu_{2-x}S$) nanostructures and their conversion to copper oxides. To our knowledge, such analysis had not been previously reported for such hierarchically mesoporous copper sulfides. Nanomaterials based on $Cu_{2-x}S$ were obtained via the solvothermal route. The structural, optical and electrochemical properties of the synthesized materials were characterized by means of X-ray diffraction (XRD), scanning electron microscopy (SEM), ultraviolet–visible (UV–Vis) spectrometry and Fourier transform infrared spectroscopy (FTIR). The influence of temperature on the shape and phase composition was analyzed by TG/DSC, XRD and FTIR in situ measurements, over the temperature range of 25–800 °C.

Materials and methods

Synthesis

All chemicals used in the study were commercially available and of analytical grade. Anhydrous $CuCl_2$ was purchased from Fisher. Thiourea (CH_4NS_2) and absolute ethyl alcohol were purchased from Avantor (Poland), while polyvinylpyrrolidone (PVP) was purchased from Sigma-Aldrich.

A schematic illustration of the synthesis procedure is presented in Fig. 1. In a typical reaction, copper chloride in various amounts (6.5 g, 7.2 g, and 2 g) was dissolved in 160 ml of absolute ethanol to form a blue solution, and then 1.6 g of thiourea was added. As a surfactant, 1 g of PVP was applied. After mixing for 30 min at room temperature, the solution was transferred to a Teflon-lined autoclave and kept sealed for 6 h at a temperature of 160 and 200 °C. Finally, the color product was collected via centrifugation, rinsed several times with anhydrous ethanol and distilled water, and then dried in a vacuum oven over 60 °C for 12 h.

Characterization techniques

The phase and crystal nature of the obtained copper sulfides were studied by means of the powder X-ray diffraction technique (X'Pert MPD diffractometer, Phillips). Phase identification was performed with the use of the X'Pert HighScore Plus software and the PDF database.

The surface morphology and chemical composition of the nanostructures were characterized using the Nova NanoSEM 200 scanning electron microscope (FEI) equipped with an EDX source and the FEI Tecnai TF X-TWIN transmission electron microscope.

Mid-infrared spectroscopic (MIR) studies were carried out to determine the structure of the obtained materials. The standard KBr pellet method was used; 128 scans were performed with a resolution of 4 cm^{-1} and over the range of 4000–400 cm^{-1} using the Bruker Vertex 70v spectrometer.

Fourier transform infrared spectroscopy (FTIR) temperature studies were carried out to determine the structure of the obtained materials, by using Harrick Scientific "Praying Mantis" DRIFTS attachment combined with a high-temperature reaction chamber. Kubelka–Munk spectra were recorded with 64 scans in 10 degree intervals. Standard MIR (middle infrared range) was used (4000–400 cm^{-1}) and a 4 cm^{-1} resolution.

The optical properties of the powders were analyzed based on the spectral dependence of total reflectance measured with a UV–Vis–NIR Jasco V-670 equipped with a 150-mm integrating sphere. Thermogravimetry (TG) and differential scanning calorimetry (DSC) analyses were

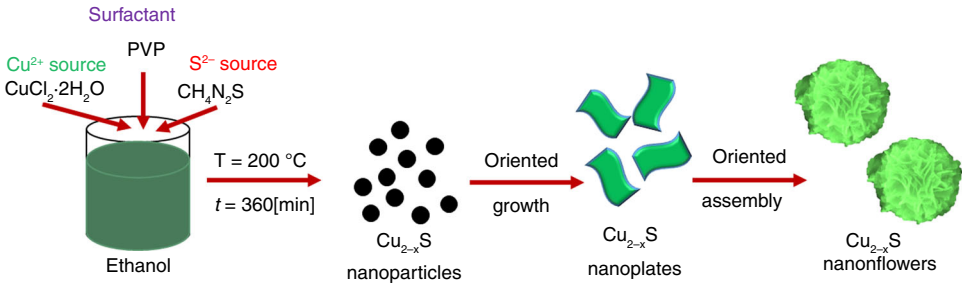

Fig. 1 A scheme illustrating the procedure of copper sulfide nanoflowers synthesis

carried out by NETZCH STA 449 F5 Jupiter in the range of 20–700 °C. The samples of mass around 25 mg were heated at a rate of 10°C min^{-1}. The measurements were taken under dynamic conditions in the synthetic air and argon atmospheres. As a reference alumina was applied.

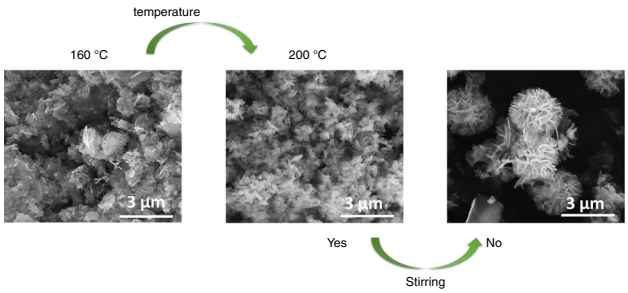

Fig. 2 Influence of conditions of hydrothermal synthesis on copper sulfide morphology

Results and discussion

Figure 2 presents the SEM images of copper sulfide structures prepared under various conditions. The tests showed that the sample (nCu:nS = 1: 1.8) obtained at 160 °C with continuous stirring was in the form of elongated nanoneedles. Raising the temperature to 200 °C had no influence on the shape of the nanostructures. It is believed that the self-assembly of many elongated grains was prevented by a mechanical factor. The ideal flower-like nanostructures were obtained in the static process. The average particle diameter was about 2–3 µm.

To study the morphological changes and evolution process, the experiments were performed at different copper-to-sulfur molar ratios. Figure 3 presents the SEM images of the obtained nanostructures. For an nCu:nS ratio of 1:1.8, geometrically symmetrical, spherical flower-like nanomaterials were fabricated. However, when the molar ratio was 2:1 or 1.8:1, the synthesis resulted in the

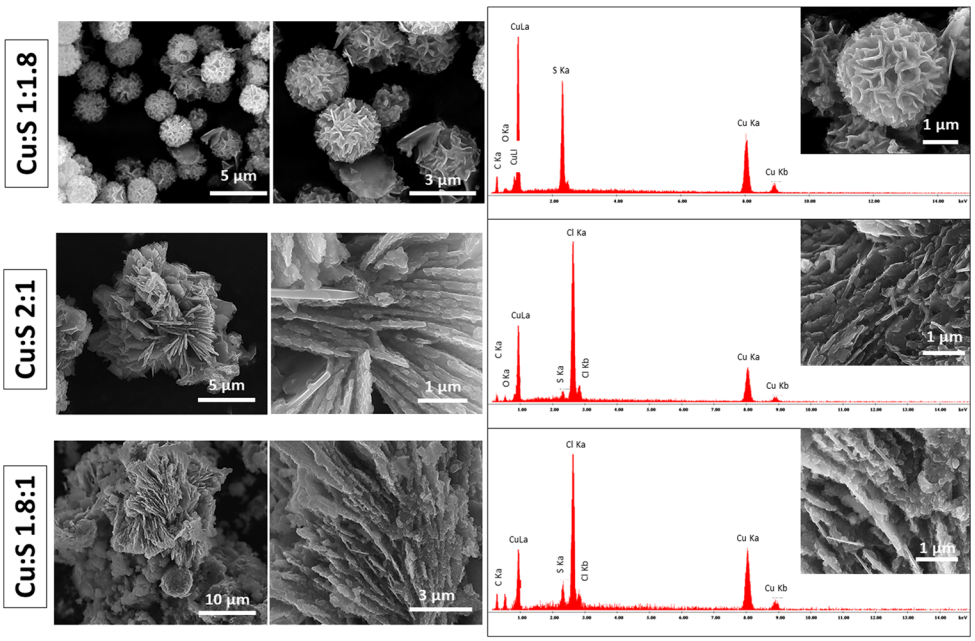

Fig. 3 SEM images and EDX spectra of copper sulfide obtained for different copper-to-sulfur molar ratios

Table 1 The at.% of elements by means of EDX analysis

Element	at.% for sample: nCu: nS		
	1:1.8	2:1	1.8:1
Cu	64.96	42.22	49.67
S	31.13	2.78	4.76
O	1.21	7.30	32.85
Cl	–	47.70	12.72

formation of a large, modified flower-like form. At higher magnification, flake graininess can be observed.

The composition and the purity of the obtained nanomaterials were evaluated by EDX analysis as shown in Fig. 3. In case of ideal spherical flower-like copper sulfide only the Cu, S and O can be observed in the spectrum. The atomic quantification of these elements (Table 1) suggests that the sample is composed of copper and sulfur, with a composition close to the stoichiometry of Cu_2S. The oxygen presence could be assigned to the partial oxidation of the structure and formation of sulfates.

When the nCu:nS molar ratio was different than 1:1.8, the EDX spectrum revealed a more complicated structure. Based on the EDX peaks associated with C, S, O and Cl, it can be concluded that the copper sulfide materials exhibited a non-stoichiometric character in this case.

According to Zhang et al. [9] solution prepared with thiourea releases more sulfur ions to react with Cu^{2+} to form CuS. The disturbed proportion of nCu:nS affects the formation mechanism of copper sulfide in the following reactions:

$$CuCl_2 + 2CS(NH_2)_2 \rightarrow 2CuCl \downarrow + C_2S_2N_4H_6 + 2HCl \quad (1)$$

$$CuCl + nCS(NH_2)_2 + \frac{1}{2}H_2O \rightarrow [Cu\{CS(NH_2)_2\}_n]Cl * \frac{1}{2}H_2O$$

$$[Cu\{CS(NH_2)_2\}_n]Cl \rightarrow CuS \downarrow \quad (3)$$

The amount of the oxygen compound suggests that instead of obtaining $Cu_{2-x}S$, there is a higher probability of receiving oxygen-based compounds such as copper oxides, sulfates or oxy-sulfates. The ratio O:S increases with an increasing amount of copper ions in the solution. Moreover, the contribution of these elements suggests that a significant amount of the copper chloride used during the synthesis remained unchanged.

XRD analyses were conducted to examine the composition and phase of the obtained nanostructures. The XRD patterns are presented in Fig. 4a. The samples with a spherical flower-like architecture contained two components, namely $Cu_{1.8}S$ (PDF-00-047-1748) and covelline (CuS) (PDF-00-006-0464). In spite of fixing the nCu:nS molar ratio at 1:1.8, it was not possible to obtain a single-phase material in the form of either pure CuS or chalcocite (Cu_2S).

The reason for this may be the formation of a cation vacancy and the stability of the compound under the applied conditions [32]. Nevertheless, the results obtained are consistent with those derived from EDX analyses.

In order to gain insight into the structure of non-stoichiometric powders, FTIR spectrometric analysis was performed. The obtained data are presented in Fig. 4b. In

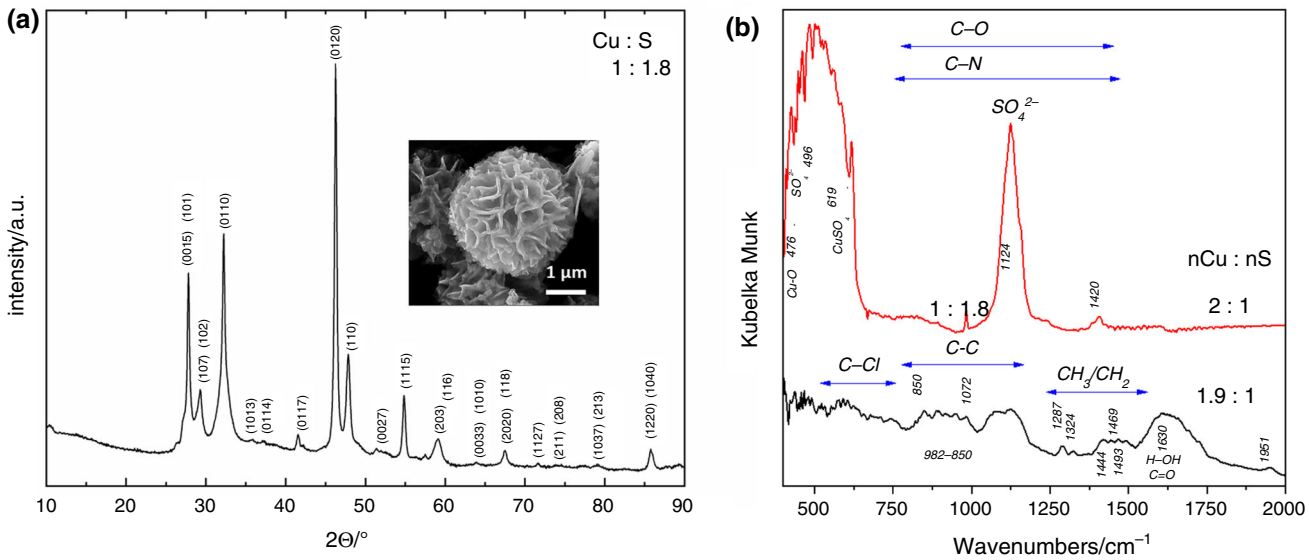

Fig. 4 X-ray diffraction patterns (black hkl planes—$Cu_{1.8}S$; red hkl planes—CuS) of $Cu_{2-x}S$ nanostructures (**a**) and FTIR spectra of non-stoichiometric powders (**b**)

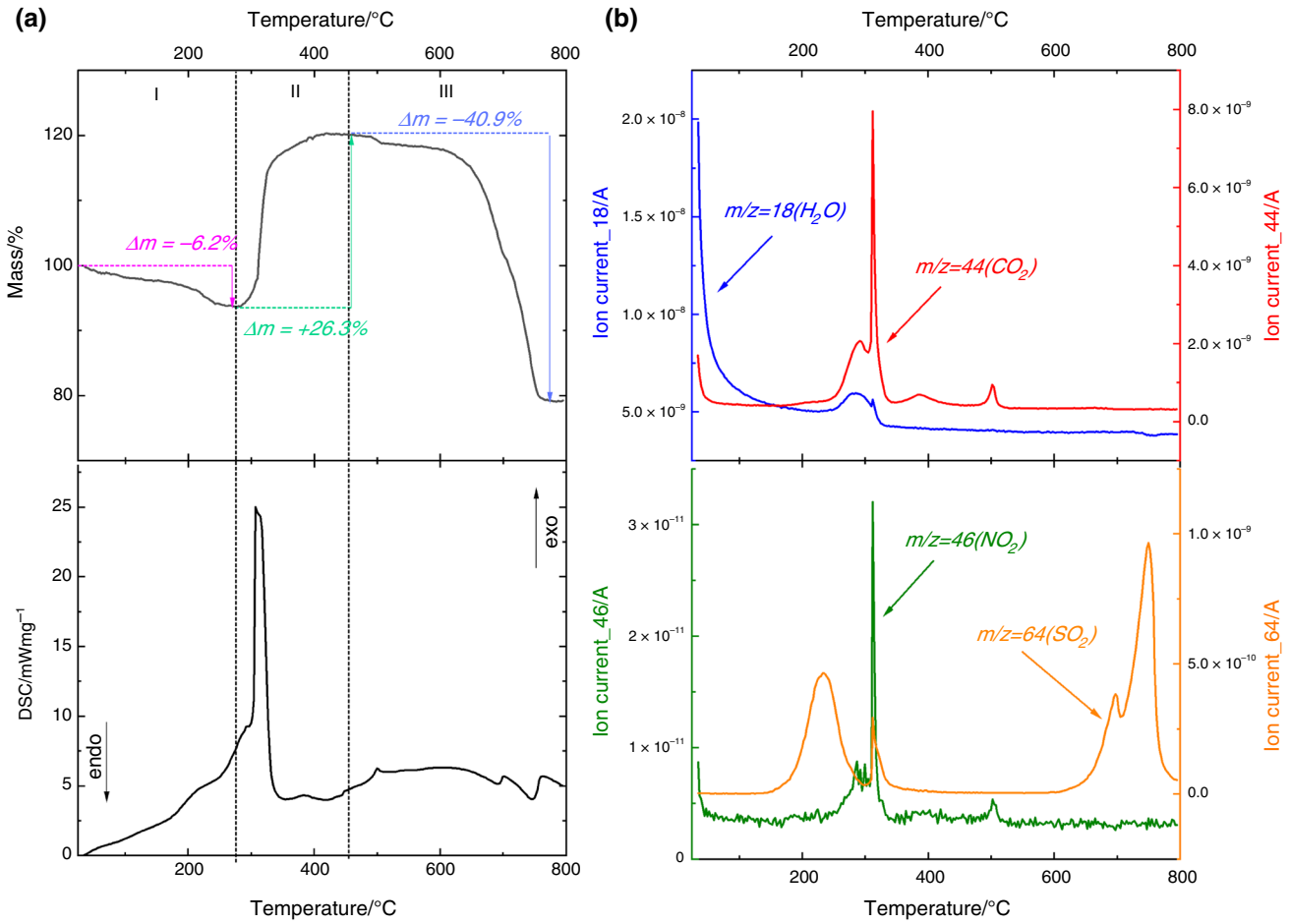

Fig. 5 Simultaneous TG/DSC (**a**) and mass spectroscopic (MS) curves (**b**) as a function of temperature for nCu:nS 1:1.8 powder

the case of nCu:nS of 2:1, the spectra show a peak at 476 cm^{-1} that is specific to Cu–O vibrations [33]. Moreover, for all measured samples, bands attributed to copper sulfate (619 cm^{-1}) and the SO_4^{2-} group (496 and 1124 cm^{-1}) are visible [34–36]. In addition, modes assigned to the residue of the precursor are present. The obtained results are highly consistent with the performed EDX analysis and confirm the multiphase composition of the investigated materials. Therefore, for further investigation only well-defined flower-like structure with composition nCu:nS 1:1.8 was taken.

In order to design particles with different anisotropic compositions sample was subjected to thermal oxidation. The first stage of the research included the TG/DSC analysis in the temperature range from 25 to 800 °C.

The obtained results are presented in Fig. 5a, b. Thermogram consists of three main regions. At first stage up to 280 °C a mass loss of about 6% is observed. According to the mass spectrometry mass changes can be related to the loss of surface-adsorbed water and to degradation of residues from organic surfactant used during solvothermal synthesis. Moreover, in this range of the temperature the roasting of sulfides may take place [19, 22–25, 28, 37, 38]. In one of the first studies conducted by Lemmerling and van Tiggelen [39, 40] it was found that adsorbed oxygen diffuses in the sulfide lattice affecting the structure rearrangement and formation of copper sulfate according to the equation:

$$CuS + 2O_2 = CuSO_4 \quad (4)$$

Further investigation by Razouk et al. [22, 38] confirmed by thermogravimetric analysis simultaneous formation of $CuSO_4$, but also suggested that mass loss can be also assigned to dissociation process of CuS followed by the sulfur oxidation:

$$2CuS = Cu_2S + S \quad (5)$$

$$S + O_2 = SO_2 \quad (6)$$

$$2CuS + O_2 = Cu_2S + SO_2 \quad (7)$$

Herein, flower-like nanostructures are composed of a mixture of CuS and Cu_9S_5. The presence of the non-stoichiometric copper sulfides increases the probability of reactions 6 and 7. It can be confirmed by the analysis of the

mass spectroscopy of the resulting gas products. An increased amount of sulfur oxides can be seen in Fig. 5b as m/z = 64 ion current line.

Above 280 °C (stage II) a significant increase in the sample mass is observed. Most of $Cu_{1.8}S$, CuS and $CuSO_4$ can react with air and form among others copper sulfate hydroxide hydrate and copper sulfate hydroxide until the temperature reaches 450 °C [21, 26, 37, 40]. Schematically, it can be written as follows:

$$2Cu_2S + 2CuSO_4 + \frac{9}{2}O_2 + 7H_2O \rightarrow Cu_3(SO_4)_2(OH)_2 * 4H_2O + Cu_3(SO_4)(OH)_4 + SO_2 \quad (8)$$

$$Cu_3(SO_4)_2(OH)_2 * 4H_2O + Cu_3(SO_4)(OH)_4 \rightarrow Cu_2OSO_4 + 4CuO + 7H_2O + 2SO_2 + O_2 \quad (9)$$

$$2Cu_2S + \frac{9}{2}O_2 \rightarrow 2CuSO_4 + Cu_2O \quad (10)$$

A sharp endothermic peak at DSC (about 300–320 °C, Fig. 5a) curve together with m/z = 46 and m/z = 44 ion current lines corresponds to the final degradation of organic residues of PVP in the form of NO_2 and CO_2. Between 400 and 500 °C almost a plateau in sample mass can be observed.

Then, at approximately 450 °C, sample mass decreases until the temperature reaches 750 °C. Copper sulfate hydroxides and their hydrates formed during annealing are converted to copper oxide sulfate and copper oxides [22, 24, 25, 37, 38]:

$$Cu_2OSO_4 = 2CuO + SO_2 + \frac{1}{2}O_2 \quad (11)$$

$$5CuSO_4 + 3CuS = 4Cu_2O + 8SO_2 \quad (12)$$

$$2CuSO_4 + Cu_2S = 2Cu_2O + 3SO_2 \quad (13)$$

$$2Cu_2O + O_2 = 4CuO \quad (14)$$

$$Cu_2S + 2O_2 = 2CuO + SO_2 \quad (15)$$

Above 750 °C sample is completely converted to CuO.

To make a thorough analysis of the changes taking place in the temperature range from room temperature to 500 °C, FTIR in situ temperature studies were carried out. Collected data are presented in Fig. 6.

In the temperature between 25 and 200 °C, spectra show no vibrations band, which suggests that the bonds present in the material are inactive in this range of infrared region. Above 200 °C bands attributed to copper sulfate (617 cm^{-1}) and the SO_4^{2-} group (1109 cm^{-1}) are visible [34–36]. According to Eq. (1) in this temperature range formation of $CuSO_4$ takes place. Then, at approximately 300 °C a wide band at 400–500 cm^{-1} with maximum at about 485 cm^{-1} specific to Cu–O vibrations [33] appears. The obtained results are highly consistent with the performed TG analysis and confirm that oxidation process starts above 200 °C.

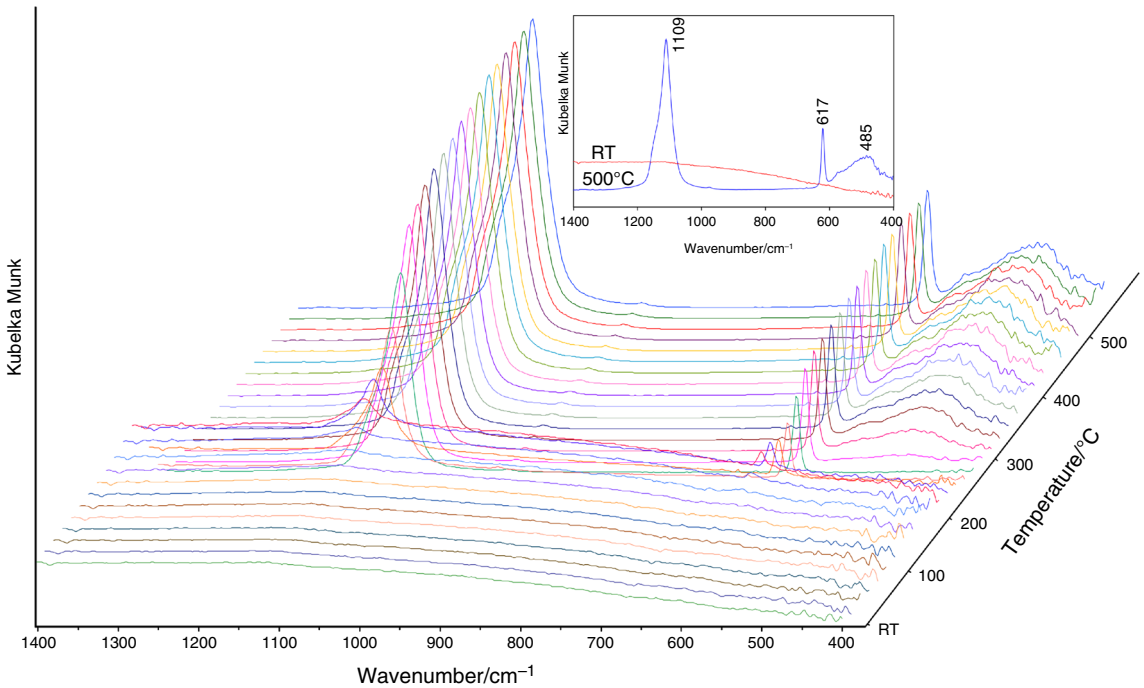

Fig. 6 FTIR temperature studies of nCu:nS 1:1.8 flower-like structure in the range of RT to 500 °C, in steps of 20 °C

In order to design particles with anisotropic composition flower-like nanopowders were annealed in air at three temperatures 200 °C, 500 °C and 700 °C for 30 min in the oven. Figure 7 presents the XRD patterns of pristine nCu:nS 1:1.8 and heated powders.

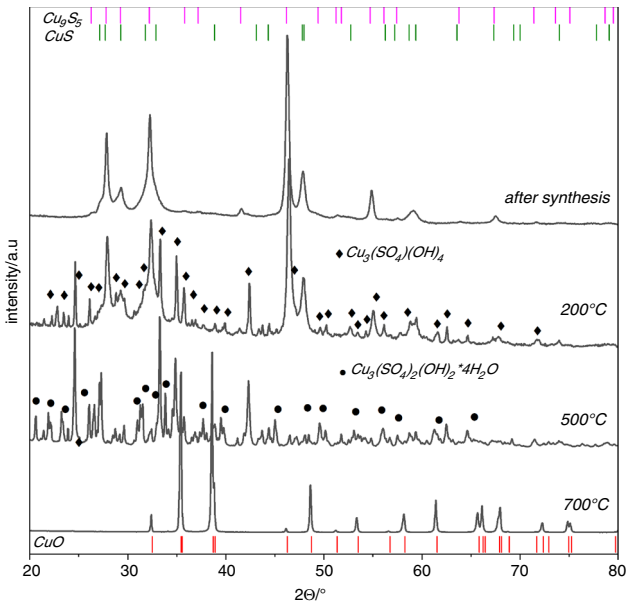

Fig. 7 XRD patterns of flower-like structure (nCu:nS 1:1.8) annealed at various temperatures in air

After synthesis a spherical flower-like architecture contained two components, namely Cu_9S_5 (PDF-00-047-1748) and covelline (CuS) (PDF-00-006-0464). Annealing at 200 °C affects reaction with oxygen water adsorbed at the surface, resulting in the formation of copper sulfate hydroxide (PDF-00-084-2037), which is in good correlation with TG measurements, Eq. (8). An increase the temperature to 500 °C causes further transformation of $Cu_{1.8}S$ to CuS and the formation of copper sulfate hydroxide hydrate ($Cu_3(SO_4)_2(OH)_2$*$4H_2O$, PDF-00-037-0525). With reference to the foregoing thermogravimetry measurements, it is clearly seen that mass increase during heating is related to the formation of more complex structures. The final stage of oxidation carried out at 700 °C indicates the formation of pure copper oxide, CuO (PDF-00-048-1548). It can be supposed that reactions 6–12 take place in the temperature range of 500–700 °C and their reaction rate is high.

Optical properties were measured using UV–Vis spectrophotometry. Figure 8 shows the reflectance spectra (%R) of the obtained nanostructures at different annealing temperatures.

The visible region band gap for well-defined flower-like nanostructures is indicative of potential applications in the field of photocatalysis. The analysis of R (λ) indicates the presence of the fundamental absorption edges in the UV–Vis range of light for sample nCu:nS 1:1.8. The analysis of the spectrophotometric data was based on the Kubelka–

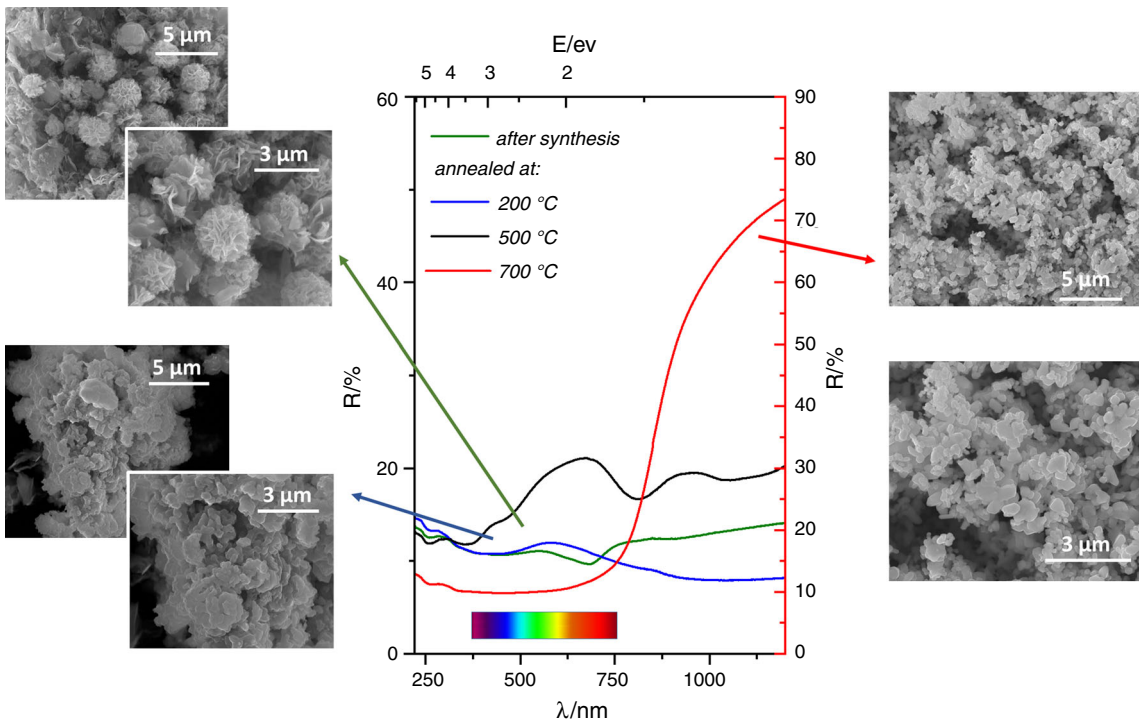

Fig. 8 Reflectance spectra and corresponding SEM images of flower-like structure (nCu:nS 1:1.8) annealed at various temperatures in air

Munk model. This approach allows the determination of effective absorption, assuming that scattering is independent of wavelength over this narrow range. The band gap energy (Eg) was calculated based on the Kubelka–Munk function $(KMh\nu)^{1/\gamma}$. The coefficient $\gamma = 2$ correspond to the indirect allowed transitions. Band gap energy values of about 2.2 and 2.8 eV obtained in the case of copper sulfide (nCu:nS; 1:1.8) remain in very good agreement with Eg for Cu_2S and CuS, respectively [18]. In the case of non-stoichiometric materials, blueshift in the UV–Vis spectra can be observed, which alters the band gap values. After annealing at 700 °C calculated band gap energy is approximately 1.47 eV and corresponds to the CuO phase. In the case of flower-like structure (nCu:nS 1:1.8) annealed at 500 °C two contributions to the electronic transition are observed. The higher one corresponds to the band gap energy of copper sulfate hydroxide (2.0–2.1 eV), while the lower one is that of CuO phase (1.40 eV).

It is worth highlighting that the band gap of copper sulfide-based nanostructures strongly depends not only on composition but also on changes in size and shape. SEM analysis of annealed powder indicates that the flower-like form is stable up to 200 °C. Applying higher temperatures affects the solubility of the material and inflicts structural damage, resulting in the formation of dense oval particles with size of up to 200 nm.

Conclusions

The synthesis of copper sulfide-based nanomaterials was performed. A certain copper-to-sulfur molar ratio was found to be a prerequisite for obtaining well-defined spherical flower-like architecture. For nCu:nS molar ratios different than 1:1.8, copper sulfide materials were found to exhibit a more complex phase structure with a non-stoichiometric character. Results of thermal analysis of oxidation process for flower-like copper sulfides, including the mechanism of oxidation processes, were defined. Obtained nanomaterials in a hierarchically mesoporous shape and molar composition of nCu:nS 1:1.8 remain stable until the temperature reaches 200 °C. Anisotropic phase composition was confirmed by XRD, FTIR and TG measurements. The controlled transformation process can affect the obtaining of semiconductor materials with unique properties. Therefore, based on the research done, it can be concluded that partial oxidation could be a powerful tool in the design of functional materials, especially for photocatalytic applications.

Acknowledgements The study was financed by the National Science Centre, Poland, as part of Project Number 2016/23/D/ST8/00024.

References

1. Fujishima A, Honda K. Electrochemical photolysis of water at a semiconductor electrode. Nature. 1972;238:37–8.
2. Isaifan RJ, Samara A, Suwaileh W, Johnson D, Yiming W, Abdallah AA, et al. Improved self-cleaning properties of an efficient and easy to scale up TiO_2 thin films prepared by adsorptive self-assembly. Sci Rep. 2017;7:1–9.
3. Lee S-K, Mills A. Detoxification of water by semiconductor photocatalysis. Science. 2004;10:173–87.
4. Natarajan S, Bajaj HC, Tayade RJ. Recent advances based on the synergetic effect of adsorption for removal of dyes from waste water using photocatalytic process. J Environ Sci. 2018;65:201–22.
5. Chen JS, Tan YL, Li CM, Cheah YL, Luan D, Madhavi S, et al. Constructing hierarchical spheres from large ultrathin anatase TiO_2 nanosheets with nearly 100% exposed (001) facets for fast reversible lithium storage. J Am Chem Soc. 2010;132:6124–30.
6. Hong Y, Tian C, Jiang B, Wu A, Zhang Q, Tian G, et al. Facile synthesis of sheet-like ZnO assembly composed of small ZnO particles for highly efficient photocatalysis. J Mater Chem A. 2013;1:5700–8.
7. Umadevi M, Jegatha Christy A. Synthesis, characterization and photocatalytic activity of CuO nanoflowers. Spectrochim Acta Part A. 2013;109:133–7.
8. Huang S, Chen C, Tsai H, Shaya J, Lu C. Photocatalytic degradation of thiobencarb by a visible light-driven MoS_2 photocatalyst. Sep Purif Technol. 2018;197:147–55.
9. Zhang YQ, Zhang BP, Ge ZH, Zhu LF, Li Y. Preparation by solvothermal synthesis, growth mechanism, and photocatalytic performance of CuS nanopowders. Eur J Inorg Chem. 2014;2014:2368–75.
10. Ai Z, Zhao G, Zhong Y, Shao Y, Huang B, Wu Y, et al. Phase junction CdS: high efficient and stable photocatalyst for hydrogen generation. Appl Catal B Environ. 2018;221:179–86.
11. Qu D, Liu J, Miao X, Han M, Zhang H, Cui Z, et al. Peering into water splitting mechanism of g-C_3N_4-carbon dots metal-free photocatalyst. Appl Catal B Environ. 2018;227:418–24.
12. Goble RJ. The relationship between crystal structure, bonding and cell dimensions in the copper sulfides. Can Mineral. 1985;23:61–76.
13. Lukashev P, Lambrecht WRL, Kotani T, van Schilfgaarde M. Electronic and crystal structure of Cu2-xS: full-potential electronic structure calculations. Phys Rev B. 2007;76:195202.
14. Baláž M, Dutková E, Bujňáková Z, Tóthová E, Kostova NG, Karakirova Y, et al. Mechanochemistry of copper sulfides: characterization, surface oxidation and photocatalytic activity. J Alloys Compd. 2018;746:576–82.
15. Xu H, Jia F, Ai Z, Zhang L. A general soft interface platform for the growth and assembly of hierarchical rutile TiO_2 nanorods spheres. Cryst Growth Des. 2007;7:1216–9.
16. Du J, O'Reilly RK. Anisotropic particles with patchy, multicompartment and Janus architectures: preparation and application. Chem Soc Rev. 2011;40:2402–16.
17. Glotzer S, Solomon M. Anisotropy of building blocks and their assembly into complex structures. Nat. Mater. 2007;n6:557–62.

18. Roy P, Srivastava SK. Nanostructured copper sulfides: synthesis, properties and applications. CrystEngComm. 2015;17:7801–15.
19. Wang S, Huang Q, Wen X, Li X, Yang S. Thermal oxidation of Cu2S nanowires: a template method for the fabrication of mesoscopic CuxO (x = 1,2) wires. Phys Chem Chem Phys. 2002;4:3425–9.
20. Nafees M, Ikram M, Ali S. Thermal behavior and decomposition of copper sulfide nanomaterial synthesized by aqueous sol method. Dig J Nanomater Biostruct. 2015;10:635–41.
21. Ramakrishna Rao VVVNS, Abraham KP. Kinetics of oxidation of copper sulfide. Metall Trans. 1971;2:2463–70.
22. Razouk RI, Farah MY, Mikhail RS, Kolta GA. The roasting precipitated copper sulphide. J Appl Chem. 1962;12:190–6.
23. Jayaweera SAA, Moss JH, Wearmouth A. Formation and reactivity of copper sulphide. Part II. Oxidation. Termochimica Acta. 1989;152:237–42.
24. Dunn J, Muzenda C. Thermal oxidation of covellite (CuS). Thermochim Acta. 2001;369:117–23.
25. Dunn JG, Muzenda C. Quantitative analysis of phases formed during the oxidation of covellite (CuS). J Therm Anal Calorim. 2001;64:1241–6.
26. Živković Ž, Štrbac N, Živković D, Velinovski V, Mihajlović I. Kinetic study and mechanism of chalcocite and covellite oxidation process. J Therm Anal Calorim. 2005;79:715–20.
27. Simonescu CM, Teodorescu VS, Carp O, Patron L, Capatina C. Thermal behaviour of CuS (covellite) obtained from copper-thiosulfate system. J Therm Anal Calorim. 2007;8(8):71–6.
28. Nafees M, Ali S, Rasheed K, Idrees S. The novel and economical way to synthesize CuS nanomaterial of different morphologies by aqueous medium employing microwaves irradiation. Appl Nanosci. 2012;2:157–62.
29. Wu C, Yu SH, Chen S, Liu G, Liu B. Large scale synthesis of uniform CuS nanotubes in ethylene glycol by a sacrificial templating method under mild conditions. J Mater Chem. 2006;16:3326–31.
30. Samsonov VM, Bembel AG, Kartoshkin AYu, Vasilyev SA, Talyzin IV. Molecular dynamics and thermodynamic simulations of segregation phenomena in binary metal nanoparticles. J Therm Anal Calorim. 2018;133:1207–17.
31. Parakhonskiy BV, Gorin DA, Baumler H, Skirtach AG. Temperature rise around nanoparticles. J Therm Anal Calorim. 2017;127:895–904.
32. Wei S-H, Xu Q, Huang B, Zhao Y, Yan Y, Noufi R. Stability and electronic structure of Cu_xS solar cell absorbers. Appl Phys Lett. 2012;100:000118–20.
33. Debbichi L, Marco de Lucas MC, Pierson JF, Krüger P. Vibrational properties of CuO and Cu_4O_3 from first-principles calculations, and Raman and infrared spectroscopy. J Phys Chem C. 2012;116:10232–7.
34. Dos Santos CC, Viali WR, Da Silva Nunes E, De Assis DR, Amantéa BE, Júnior MJ. Aqueous nanofluids based on copper MPA: synthesis and characterization. Mater Res. 2017;20:104–10.
35. Berger J. Infrared and Raman spectra of $CuSO_4$, $5H_2O$; $CuSO_4$, 5D2O; and CuSeO, $5H_2O$. J Raman Spectrosc. 1976;5:103–14.
36. Arun KJ, Batra AK, Krishna A, Bhat K, Aggarwal MD, Joseph Francis PJ. Surfactant free hydrothermal synthesis of copper oxide nanoparticles. Am J Mater Sci. 2015;5:36–8.
37. Kundu J, Pradhan D. Influence of precursor concentration, surfactant and temperature on the hydrothermal synthesis of CuS: structural, thermal and optical properties. New J Chem. 2013;37:1470.
38. Razouk RI, Kolta GA, Mikhail RS. The roasting of copper sulphides. II. Natural copper sulphides. J Appl Chem. 1965;15:191–6.
39. Lemmerling J, van Tiggelen A. Contribution a l'etude des reactions entre gaz et solides II Oxidation sulfatante de sulfures precipites. Bull Soc Chim Belg. 1955;64:470–83.
40. Lefevre MM, Lemmerling J, van Tiggelen A. Sur quelques reactions dans le grillage de sulfures precipites. Bull Soc Chim Belg. 1956;65:580–95.